

Investigation of the effect of Abemaciclib on breast cancer spheroids in a three-dimensional (3D) environment

Can Sürücüoğlu , Selen Oztürk , Aysun Kılıç Süloğlu* 

¹Hacettepe University, Faculty of Science, Department of Biology, Zoology Section, Beytepe Campus, Ankara, 06800, Türkiye

Article History

Received 31 October 2025

Accepted 16 April 2026

First Online 8 May 2026

Corresponding Author

Tel.: +90 312 297 61 24

E-mail: aykilig@hacettepe.edu.tr

Keywords

Abemaciclib,
MDA-MB-231
Breast cancer
Tumor spheroid
3D Petri Dish®

Copyright

This is an open-access article distributed under the terms of the [Creative Commons Attribution 4.0 International License \(CC BY\)](https://creativecommons.org/licenses/by/4.0/).

Abstract

Breast cancer is a leading cause of cancer-related mortality worldwide, with triple-negative breast cancer (TNBC) representing the most aggressive subtype due to its lack of targetable receptors and poor prognosis. Abemaciclib, a selective cyclin-dependent kinase 4 and 6 (CDK4/6) inhibitor, has emerged as a promising therapeutic agent by blocking cell-cycle progression and limiting tumor proliferation.

To better mimic tumor architecture, this study employed spheroids of the TNBC cell line MDA-MB-231 generated with the three-dimensional (3D) Petri Dish® system. The cytotoxic effects of Abemaciclib were evaluated in comparison with Doxorubicin under both two-dimensional (2D) monolayer and three dimensional (3D) spheroid culture conditions using an MTS-based cell viability assay. Complementary analyses included immunofluorescence staining of filamentous actin (F-actin) to assess cytoskeletal alterations, and flow cytometry to determine cell-cycle distribution.

Within the tested concentration ranges, spheroids showed reduced sensitivity to Abemaciclib compared with monolayers, indicating that 3D culture conditions may influence drug penetration and adaptive resistance. Abemaciclib suppressed proliferation in a concentration-dependent manner by altering cell-cycle distribution, with G0/G1 accumulation at lower concentrations and G2/M accumulation at higher concentrations, accompanied by a reduced S-phase fraction.

These findings highlight the relevance of 3D models for preclinical drug evaluation and support the therapeutic potential of Abemaciclib in aggressive breast cancer.

Introduction

Breast cancer is one of the most prevalent malignancies and remains a leading cause of cancer-related mortality among women globally (Blowman et al., 2018). According to the World Cancer Report, approximately 2.1 million new cases and 627,000 breast cancer-related deaths occur annually (Wild et al., 2020). This clinical burden underscores the need for accurate subtype classification to support effective diagnosis and treatment.

Accurate classification of breast cancer subtypes is crucial because it enables appropriate strategies for the early diagnosis and treatment (Scope et al. 2017; Zhang, 2023). Breast cancer is classified based on the expression status of biomarkers such as estrogen receptor (ER), progesterone receptor (PR), human

epidermal growth factor receptor-2 (HER-2), and proliferation marker protein Ki-67 (Sørli et al. 2001). Triple-negative breast cancer (TNBC) is characterized by lack of ER and PR expression and absence of HER2 overexpression/amplification and accounts for approximately 15% of breast cancer cases (Merino Bonilla et al., 2017; McGuire et al., 2017). Characterized by a basal-like gene signature, high frequency of BRCA1/2 mutations, and a tendency for early metastasis, TNBC remains the most aggressive subtype with limited targeted treatment options, often necessitating a treatment paradigm reliant on chemotherapy (Merino Bonilla et al. 2017; McGuire et al. 2017).

The MDA-MB-231 cell line is a widely used model of TNBC and exhibits aggressive and invasive properties ([Lehmann et al. 2011](#)). Due to these characteristics, the MDA-MB-231 cell line is utilized in various research areas, including the study of metastasis, drug resistance, immune evasion, tumor behavior in three-dimensional (3D) microenvironments, and spheroid cultures ([Bonnier et al., 2015](#)).

Targeting cell-cycle regulation is an important strategy in cancer therapy. Cyclin-dependent kinases 4 and 6 (CDK4/6) play a key role in the transition from the G1 phase to the S phase of the cell cycle, and dysregulated growth signals in cancer cells activate these proteins ([Guney Eskiler et al., 2022](#)). While triple-negative breast cancer (TNBC) has historically been associated with a high frequency of Retinoblastoma (Rb) tumor suppressor loss ([Parinyanitikul et al., 2019](#)), recent studies indicate that 35% to 50% of primary TNBC tumors retain Rb expression ([Goel et al., 2025](#)). Furthermore, specific molecular subsets, such as the luminal androgen receptor (LAR) subtype, are predominantly Rb-wild type and have demonstrated sensitivity to CDK4/6 inhibition ([Chica-Parrado et al., 2024](#)). This retention of functional Rb provides a strong biological rationale for evaluating CDK4/6 inhibitors in this context. Abemaciclib, as a selective inhibitor of CDK4/6, inhibits the phosphorylation of retinoblastoma protein (pRb), thereby arresting the cell cycle in the G1 phase and suppressing the proliferation of cancer cells ([Arslan et al., 2022](#)). Studies on Abemaciclib conducted with various MDA-MB-231 cell lines have demonstrated that it induces apoptosis in cells ([Ozman et al., 2021](#); [Inao et al., 2019](#)). Nevertheless, studies in 3D models that mimic the tumor microenvironment are limited, and investigating the properties of Abemaciclib holds critical importance in determining the role of this drug in TNBC treatment.

Two-dimensional (2D) cell cultures have long been preferred in *in vitro* studies due to their cost-effectiveness and reproducibility ([Kapałczyńska et al., 2018](#); [Jensen and Teng, 2020](#); [Wang et al., 2023](#)). However, they lack the complex cellular architecture required to fully recapitulate the *in vivo* tumor microenvironment ([Wang et al., 2014](#)). In contrast, 3D culture systems better reproduce tumor characteristics, such as cell–cell interactions, nutrient gradients, and hypoxic cores ([Habanjar et al., 2021](#)). Therefore, 3D models provide a physiologically relevant platform than 2D cultures for evaluating therapeutic efficacy and drug resistance mechanisms in aggressive breast cancers.

In this study, we established a 3D tumor spheroid model of the MDA-MB-231 cell line using the 3D Petri Dish® system to comparatively evaluate the effects of Abemaciclib in 2D and 3D environments. Specifically, we assessed drug response through cell viability assays (using Doxorubicin as a positive control), analyzed cell-cycle distribution via flow cytometry, and evaluated cytoskeletal alterations using F-actin immunofluorescence staining. This approach allows for

a comprehensive assessment of how the 3D spatial architecture influences drug sensitivity compared to traditional monolayers.

While Abemaciclib has been widely studied in TNBC monolayer cultures, its evaluation in 3D spheroid models—which better mimic *in vivo* drug resistance mechanisms—remains limited. By integrating viability, cell-cycle, and cytoskeletal analyses in a 3D system, this study aims to contribute to the understanding of drug penetration and the therapeutic potential of CDK4/6 inhibition in aggressive breast cancer subtypes.

Material and Methods

Materials

The reagents and materials used in this study were categorized by their application. Cell culture reagents, including Dulbecco's Modified Eagle's Medium–High Glucose (DMEM-HG) and penicillin/streptomycin, were obtained from Capricorn Scientific (Ebsdorfergrund, Germany). Fetal bovine serum (FBS) was purchased from BioWest (Nuaille, France), while trypsin/EDTA and phosphate-buffered saline (PBS) without calcium and magnesium were sourced from Thermo Fisher Scientific (Waltham, MA, USA). Trypan blue solution was used for cell counting.

For the 3D spheroid model, spheroids were generated using the 3D Petri Dish® system (MicroTissues, USA) with agarose, sodium chloride (NaCl), and RNase purchased from Sigma-Aldrich (St. Louis, MO, USA). Inhibitors and compounds included Abemaciclib (Selleckchem, Houston, TX, USA) and Doxorubicin (MedChemExpress, Monmouth Junction, NJ, USA), with dimethyl sulfoxide (DMSO) sourced from Sigma-Aldrich (St. Louis, MO, USA).

Immunofluorescence and staining reagents such as CellTracker™ dye, phalloidin Alexa Fluor® 555, and BSA Fraction V were provided by Thermo Fisher Scientific (Waltham, MA, USA). Triton X-100, methanol, paraformaldehyde, and Tween-20 were purchased from Merck (Darmstadt, Germany). Glacial acetic acid was obtained from Carlo Erba (Italy). Propidium iodide (PI) was obtained from AppliChem (Darmstadt, Germany), while DAPI and DAPI mounting medium were sourced from Abcam (Cambridge, UK).

For assays and consumables, the CellTiter 96® AQueous One Solution Cell Proliferation Assay (MTS) kit was purchased from Promega (Madison, WI, USA). Multiwell plates (6-, 12-, 48-, and 96-well) were obtained from Greiner Bio-One (Kremsmünster, Austria), and 4-well chamber slides were purchased from Merck (Darmstadt, Germany).

Cell Culture Conditions

The human triple-negative breast cancer cell line MDA-MB-231 cells (ATCC, HTB-26) were grown in DMEM medium supplemented with 10% FBS and 1% penicillin/streptomycin. The cells were cultured at 37°C in a humidified incubator with 5% CO₂, and then

passed at 70–80% confluence using trypsin/EDTA. Cell viability and density were routinely assessed by the trypan blue exclusion method.

MDA-MB-231 Spheroid Formation with 3D Petri Dish® Method

Spheroids were generated from MDA-MB-231 cells using 3D Petri Dish® system (MicroTissues, USA) (Öztürk et al., 2024). A 2% (w/v) agarose solution was prepared by dissolving 1 g agarose in 50 mL distilled water containing 0.9% (w/v) NaCl, followed by autoclaving. After cooling, 580 µL of the solution was dispensed into each Petri Dish® mold and allowed to polymerize at room temperature. The resulting agarose gels were transferred into 12-well plates and incubated with serum-free DMEM for 30 min; the medium was then removed. MDA-MB-231 cell suspensions were prepared at densities of 5×10^4 and 1×10^5 cells per agarose gel, and a volume of 100 µL of cell suspension was seeded into the seeding chamber of each gel, allowing cells to settle into the 81 micro-wells. Plates were incubated for 15 min to allow the cells to settle onto the agarose. Subsequently, 2.5 mL of serum-containing DMEM was added to each well.

Morphometric Analysis of Spheroids (Diameter and Area)

Following spheroid formation with the 3D Petri Dish® system, and prior to any drug treatment, spheroids were monitored daily for six consecutive days using an inverted microscope (Olympus CKX18, Tokyo, Japan). Three spheroids from each well were randomly selected and analyzed. Spheroid diameter (µm) and area (µm²) were quantified using cellSens software (Olympus). To determine the optimal seeding density for downstream assays, the growth profiles of spheroids initiated with 5×10^4 versus 1×10^5 cells per gel were compared. Based on the formation of compact, uniform spheroids and consistent growth metrics, the density of 1×10^5 cells per agarose gel was selected for subsequent cytotoxicity and mechanistic studies.

Drug Treatment

Abemaciclib was dissolved in DMSO to prepare a 10 mM stock solution, which was aliquoted and stored at -20 °C. Working concentrations were freshly prepared by diluting the stock in complete culture medium, ensuring that the final DMSO concentration did not exceed 0.1% (v/v). Based on preliminary toxic response assays, Abemaciclib doses were determined as 10, 20, and 25 µM for 2D experiments, while concentrations of 20, 30, and 40 µM were utilized for 3D spheroid cultures. Doxorubicin was used as a positive control. A stock solution was prepared by dissolving the powdered compound in 50 mg stock in 1 mL of DMSO to reach a stock concentration of approximately 86 mM and stored at -20 °C. For 2D monolayer experiments, drug treatments were initiated 24 h after cell seeding once the culture reached approximately 70–80% confluency.

In the 3D spheroid model, treatments were administered 24 h after the initiation of the 3D Petri Dish® system, following the successful establishment of cell aggregates. In all experimental groups, the final DMSO concentration was maintained below 0.1% (v/v) to ensure no vehicle-induced toxicity occurred. The selection of elevated dosage ranges for the 3D environment was specifically designed to account for the increased therapeutic resistance and the distinct drug penetration profile inherent to the 3D architecture.

Cell Viability Assay (MTS)

Cell viability was assessed using the CellTiter 96® AQueous One Solution kit (Promega, Madison, WI, USA) according to the manufacturer's instructions. This assay was preferred over the conventional MTT method as it provided more consistent results within the 3D spheroid architecture. For 2D cultures, MDA-MB-231 cells were suspended at 1×10^5 cells/mL and seeded into 96-well plates at 100 µL per well (1×10^4 cells/well). After incubation for 24 h at 37 °C in a 5% CO₂ incubator, the medium was carefully removed. Cells were then treated with 100 µL of fresh medium containing Abemaciclib (10, 20, and 25 µM) or the positive control Doxorubicin (5, 10, and 20 µM) for 24, 48, and 72 h. At each time point, 20 µL MTS reagent was added to each well, plates were incubated for 3 h in the dark, and then gently shaken for 5 min. Absorbance was measured at 490 nm using a microplate reader (µQuant, BioTek Instruments, USA).

For 3D cultures, a cell suspension of 1×10^6 cells/mL was prepared and incubated for 24 h to allow spheroid formation. After 24 h, spheroids in 12-well plates were treated with 2.5 mL of medium containing Abemaciclib (20, 30, and 40 µM) or Doxorubicin (20, 40, and 60 µM) for 24, 48, and 72 h. At the end of each incubation period, the medium was aspirated (leaving 100 µL for 3D samples to maintain the reagent ratio), and 20 µL of MTS reagent was added to each well. Plates were incubated for 3 h at 37 °C in the dark. Following incubation and the plates were shaken for 5 min to ensure a homogeneous distribution of the formazan product, the resulting solution was transferred to a 96-well plate to ensure accurate optical density (OD) readings. Absorbance was measured at 490 nm using a microplate reader (µQuant, BIO-TEK Instruments, Inc., Winooski, VT, USA).

The viability percentage was calculated using the following formula:

$$\% \text{ Viability} = \frac{\{\text{Treatment Group}_{OD}\}}{\{\text{Control Group}_{OD}\}} \times 100$$

The half-maximal inhibitory concentration (IC₅₀) values were calculated via regression analysis using SPSS software (IBM Corp., Armonk, NY, USA)

F-Actin Immunofluorescence Staining

MDA-MB-231 cells were seeded onto 4-well chamber slides at 1×10^5 cells in 300 µL per well. Cells were allowed to adhere for 24 h at 37 °C in a humidified 5% CO₂ incubator. Cells were then treated with

Abemaciclib at 10 and 20 μM for an additional 24 h. After treatment, the medium was removed, and cells were fixed with 4% paraformaldehyde at room temperature for 15 min. To allow for intracellular labeling, cells were permeabilized and washed three times for 2 min each with PBS containing 0.3% Triton X-100. Blocking was performed with 3% BSA for 45 min. F-actin filaments were then labeled with Phalloidin-Alexa Fluor 555 (from a 66 μM stock, 1:400; Waltham, MA, Thermo Fisher) by adding 200 μL per well and incubating for 1 h at room temperature in the dark. After staining, cells were washed three times with PBS for 2 min and mounted with a DAPI-containing mounting medium. Prepared slides were examined under an Olympus CKX18 (Tokyo, Japan) inverted microscope, and representative images were captured.

Flow Cytometry

MDA-MB-231 cells were seeded into 6-well plates at a density of 3×10^5 cells/well and left for incubation to reach appropriate density. Upon reaching sufficient density, cells were treated with Abemaciclib at concentrations of 10 and 20 μM for 48 h. To harvest the cells, Trypsin/EDTA solution was added, and plates were incubated for 3 min at 37 $^{\circ}\text{C}$. The reaction was neutralized with serum-containing medium, and the cell suspension was centrifuged at 1200 rpm for 5 min at 4 $^{\circ}\text{C}$. The supernatant was discarded, and the cell pellet was resuspended in 3 mL of PBS by vortexing. Subsequently, cells were fixed in 70% ethanol and incubated overnight at 4 $^{\circ}\text{C}$. After fixation, cells were centrifuged again (1200 rpm, 5 min, 4 $^{\circ}\text{C}$), the supernatant was removed, and the pellet was washed with 1 mL of PBS. For DNA staining, cells were incubated with 70 μL of RNase A (100 $\mu\text{g}/\text{mL}$) and 50 μL of Propidium Iodide (PI; 50 $\mu\text{g}/\text{mL}$) for 30 min at room temperature in the dark. Cell cycle distribution was analyzed by counting 15,000 nuclei per sample using a Beckman Coulter Cytoflex LX flow cytometer (USA). Data were evaluated using Multicycle software (Phoenix Flow Systems, USA) to determine the percentage of cells in the G0/G1, S, and G2/M phases.

Statistical Analysis

All statistical analyses were performed as three independent biological replicates, performed at different times using cells harvested from separate flasks. For each independent experiment, technical triplicates were performed ($n=3$). Data were expressed as mean \pm standard deviation (SD). Statistical analyses were carried out using GraphPad Prism version 10.6 (GraphPad Software, San Diego, CA, USA). Given the presence of two independent variables—drug concentration (dose group) and incubation period (24, 48, and 72 h)—a two-way analysis of variance (ANOVA) was employed to evaluate the therapeutic effects of Abemaciclib and Doxorubicin in 2D and 3D cultures. Following the two-way ANOVA, Dunnett's and Šídák's post-hoc test were applied to compare the significance

of differences between treated groups and the untreated control, and to evaluate the comparative efficacy between Abemaciclib and Doxorubicin at equivalent concentrations. The half-maximal inhibitory concentration (IC_{50}) values were calculated through nonlinear regression analysis using IBM SPSS Statistics software (IBM Corp., Armonk, NY, USA). A P value ≤ 0.05 was considered statistically significant.

Results

Spheroid Formation and Measurements

To establish the optimal protocol for spheroid formation, MDA-MB-231 cells were seeded in 3D Petri Dishes[®] system at two different densities: 5×10^4 and 1×10^5 cells per agarose gel. The formation, development, and morphological integrity of the spheroids were monitored daily for six consecutive days using an inverted microscope, and morphometric parameters (diameter and area) were quantified using the CellSense software (Olympus, Tokyo, Japan) (Figure 1). Observations revealed that the initial seeding density significantly influenced the growth kinetics of the spheroids. On Day 1, the mean spheroid diameter was 235.45 μm in the 5×10^4 cells/gel group, compared to 264.95 μm in the 1×10^5 cells/gel group. By the end of day 6, these values increased to 303.89 μm and 415.02 μm , respectively (Figure 2). Statistical analysis using an ordinary two-way ANOVA showed that both the incubation period ($P < 0.0001$) and cell concentration ($P = 0.0009$) had significant overall effects on spheroid diameter. Post-hoc multiple comparisons using Dunnett's test revealed significant growth by Day 6 relative to the Day 1 control in both groups ($P = 0.0217$ for 5×10^4 and $P < 0.0001$ for 1×10^5). Area measurements exhibited a similar trend. The initial area on day 1 was 46458.5 μm^2 for the 5×10^4 cells/gel group and 58484.21 μm^2 for the 1×10^5 cells/gel group. On the sixth day, these areas had grown to 74894 μm^2 and 131232 μm^2 , respectively (Figure 3). Both the incubation period ($P < 0.0001$) and initial cell density ($P < 0.0001$) were found to have highly significant overall effects on the spheroid area. Post-hoc analysis confirmed that by Day 6, spheroid areas in both groups were significantly larger than their Day 1 baselines ($P = 0.0230$ and $P < 0.0001$, respectively). Based on these findings, a density of 1×10^5 cells per gel was selected as the optimal condition for subsequent experiments. This concentration produced larger spheroids with superior structural integrity and a more robust 3D microenvironment, ensuring stability during the long-term drug treatment assays for Abemaciclib and Doxorubicin.

Cell Viability Assay

The viability response of MDA-MB-231 cells to Abemaciclib in both 2D and 3D cultures was comparatively evaluated, with Doxorubicin serving as a positive control. In the 2D culture, both Abemaciclib (10, 20, and 25 μM) and Doxorubicin (5, 10, and 20 μM)

reduced cell viability in a time- and concentration-dependent manner, with the strongest effect observed at the highest concentrations after 72 h ($P \leq 0.05$). The calculated IC_{50} values for Abemaciclib were consistent with this trend, ranging from 21.47 μM at 24 h to 19.32 μM at 72 h (Table 1, Figure 4). In the 3D spheroid model, however, a distinct response profile was observed. Although Abemaciclib (20, 30, and 40 μM) initially decreased spheroid viability in a concentration-dependent manner at 24 h (with viability reduced to 48.71% at 40 μM , $P \leq 0.05$), a notable recovery trend was identified at 48 and 72 h (Figure 5). Interestingly, spheroid viability increased at the 48 and 72 h indicating a time-dependent recovery. A similar pattern was observed for spheroids treated with Doxorubicin (20, 40, and 60 μM) as the incubation period was extended (Figure 5).

The IC_{50} values further quantified the therapeutic resistance of the 3D configuration. For Abemaciclib in 3D culture, the IC_{50} was determined to be 37.12 μM at 24 h. However, at the 48 and 72 h time points, the IC_{50} values were not reached within the tested concentration range (up to 40 μM) because the cell viability remained above 50% due to the observed recovery trend (Table 1). This profile suggests that the compact structure of the spheroids (1×10^5 cells/gel) restricts drug penetration and facilitates adaptive survival mechanisms in TNBC cells.

F-Actin Immunofluorescence Staining

The effects of Abemaciclib on the cytoskeletal structure of MDA-MB-231 monolayer cells were examined, specifically focusing on F-actin filaments, which provide essential mechanical support and play a critical role in maintaining cellular integrity and shape. Following 24h incubation of the cells with Abemaciclib, immunofluorescence staining was performed to visualize the F-actin filamentous structure under an immunofluorescence microscope (Figure 6). In the control group, F-actin filaments showed a relatively regular and homogeneous distribution along the cytoplasm and cell periphery, and intercellular boundaries were readily. Treatment with 10 μM Abemaciclib was associated with visible alterations in actin organization compared with controls, including thicker filamentous structures and an increased number of cellular protrusions accompanied by changes in cell morphology. In contrast, in the group treated with 20 μM Abemaciclib, F-actin signal was markedly reduced and discontinuous, with regions showing minimal or absent filamentous staining, and cell boundaries appeared less distinct with pronounced morphological disruption. Overall, these observations indicate a concentration-dependent alteration of F-actin organization in 2D MDA-MB-231 cultures following Abemaciclib exposure.

Cell Cycle Analysis Results

To determine the effects of Abemaciclib on the cell cycle, MDA-MB-231 cells were treated with the drug (10 and 20 μM) for 48 h, and their cell cycle profiles were analyzed by flow cytometry (Figure 7). The control group exhibited a balanced cell cycle distribution, with 39.55% of cells in the G0/G1 phase, 13.55% in the S phase, and 16.90% in the G2/M phase. Treatment with 10 μM Abemaciclib induced a notable arrest in the G0/G1 phase, increasing this population to 45.11%, while the S phase population decreased significantly to 8.58%. A concomitant increase in the G2/M phase (21.39%) was also observed compared to the control group. In contrast, the 20 μM Abemaciclib treatment caused a distinct shift in the cell cycle profile. At this higher concentration, the G0/G1 population decreased substantially to 19.35%, while a dramatic accumulation of cells was detected in the G2/M phase, reaching 44.05% (Figure 8). The proportion of cells in the S phase remained low, comparable to that of the 10 μM treatment group. These findings indicate that Abemaciclib induces concentration-dependent alterations in the cell-cycle distribution of MDA-MB-231 cells. Lower concentrations were associated with an increased G0/G1 fraction, consistent with CDK4/6 inhibition, whereas higher concentrations were associated with a pronounced accumulation in the G2/M fraction.

Discussion

While 2D cultures remain standard owing to their low cost and accessibility, they do not recapitulate the *in vivo* tumor microenvironment, including cell-cell and cell-matrix interactions (Wang et al., 2023). Accordingly, 3D culture systems have been increasingly adopted; the MDA-MB-231 line an invasive, basal-like TNBC model has been widely used in transwell invasion, 3D spheroid, and epithelial-mesenchymal transition (EMT) assays to interrogate drug resistance, cell behavior, and tumor-microenvironment interactions (Lehmann et al., 2011; Bonnier et al., 2015). In this study, we established MDA-MB-231 spheroids and demonstrated that initial seeding density strongly influenced spheroid size and structural integrity, with 1×10^5 cells per gel providing a consistent model. As shown in the result, seeding density-dependent spheroid growth supports the generation of robust and reproducible MDA-MB-231 spheroids in this platform for downstream drug-response assessment. Furthermore, these findings are consistent with previous studies on the growth of spheroids created using different 3D culture systems and cell concentrations. In a study consistent with ours, researchers using MDA-MB-231 cells in Geltrex®-supported 3D models in ultra-low attachment plates detected increasing diameter values over time in spheroids formed at different concentrations (Dubois et al., 2017). Similarly, in another study, Matrigel®-supported MDA-MB-231 spheroids with different cell

concentrations grew over time and achieved different sizes (Badea et al., 2019). However, in a 2022 study, Badea et al. used the hanging drop method to create MDA-MB-231 spheroids reported that although the initial diameters varied, consistent with our study, the diameters decreased as the incubation period was extended (Badea et al., 2022). These differences in spheroid growth are thought to stem from various factors, such as the diversity of methods used, different cell numbers, and experimental conditions. For instance, previous work establishing a 3D multicellular placental microtissue model using the same 3D Petri Dish TM method provides context for these variations. Specifically, co-cultured placental spheroids demonstrated a temporary decrease in diameter and area measurements on the fourth day compared to the third. This observation supports the interpretation of size variances in the MDA-MB-231 spheroids, suggesting that compaction is a physiological response common to 3D Petri Dish TM models and is reflective of increased tissue maturity (Öztürk et al., 2024). As a significant innovation, this study represents a new application of the 3D Petri® Dish system for spheroid formation using the MDA-MB-231 cell line. Furthermore, the establishment of this model provides a new and robust platform for studying the behavior of aggressive tumor cells in 3D conditions and holds significant potential as a reference for future academic and industrial drug screening studies.

In present study, it was determined that Abemaciclib application in 2D culture conditions significantly reduced the viability of MDA-MB-231 cells in a concentration- and time-dependent manner. The fact that the drug reduced cell viability to the greatest extent at the highest concentration at 72 hours underscores its potent inhibitory effect. Doxorubicin, evaluated as a positive control, similarly decreased viability in a concentration- and time-dependent fashion. The calculated IC_{50} value for Abemaciclib was determined to be 21.47 μ M. This value falls within the broad spectrum of IC_{50} concentrations reported in the literature, highlighting the variable sensitivity of MDA-MB-231 cells to Abemaciclib. In a study by Anwer et al. (2022) investigating the effects of Abemaciclib-loaded nanosponges on MCF-7 and MDA-MB-231 cells, the IC_{50} value of Abemaciclib in MDA-MB-231 cells was reported to be approximately 36.7 μ M. In another study investigating the effects of sodium butyrate and Abemaciclib on MDA-MB-231 cells, the IC_{50} value of Abemaciclib was determined to be 14.55 μ M, which dropped to 2.55 μ M in combination therapy (Elnozahi et al., 2022). In two studies from 2025, IC_{50} values were reported as 32 μ M and 18.02 μ M, respectively (Sharaky et al., 2025; He et al., 2025). This variability in data is thought to stem from different methodologies, including experimental conditions such as cell seeding density, incubation time, and the use of different formulations, as well as variables related to cell line subpopulations. Our study supports Abemaciclib's

antiproliferative activity in MDA-MB-231 cells under standard 2D culture conditions and emphasize the importance of experimental context when comparing IC_{50} values across studies.

In 3D culture conditions of the MDA-MB-231 cell line, the application of Abemaciclib at concentrations of 20, 30, and 40 μ M revealed a significant decrease in spheroid viability after 24 h of treatment; however, higher viabilities was observed at 48 and 72 h incubation periods. This pattern can be described as an attenuation of the initial decrease over time rather than definitive evidence of acquired resistance, because time-dependent changes in MTS readouts in 3D architectures can reflect a combination of biological adaptation and assay-related factors. Although Doxorubicin, used as a positive control, similarly reduced cell viability, the higher cytotoxic effect of Abemaciclib at the same concentrations highlights the potential efficacy of this drug on triple-negative breast cancer cells. The IC_{50} value calculated for the 3D model in our study is 37.126 μ M. Importantly, this value corresponds to the 24 h time point (where it falls within the tested range). At 48 and 72 h, 50% inhibition was not reached within the tested Abemaciclib concentration range (up to 40 μ M); therefore, IC_{50} values at these later time points are reported in Table 1. An expanded dose panel would be required to obtain within-range IC_{50} estimates at later time points. However, in a 2025 study, Nehme et al. investigated the effects of Abemaciclib solely through a fluorescent staining method (Nehme et al., 2025). Comparatively, in studies conducted on Palbociclib, another CDK4/6 inhibitor, IC_{50} values of 29.7 μ M and 29.69 μ M have been reported in similar 3D models (Velez et al., 2022; Doello, 2021). These comparisons provide context for cross-compound evaluation, although pharmacodynamic differences and experimental design can contribute to variability (George et al., 2021). This observed resistance is consistent with findings that 3D models more realistically reflect the *in vivo* tumor microenvironment and thus exhibit a stronger defense against therapeutic agents (Sant & Johnson, 2017).

Within spheroids, contact-mediated signaling arising from intercellular and cell-matrix interactions augments pro-survival pathways (Olive & Durand, 1994). The layered architecture imposes diffusion barriers that create central hypoxia and nutrient deprivation, driving cells into G0/G1 quiescence and diminishing the efficacy of Abemaciclib (Minchinton & Tannock, 2006; Imamura et al., 2015). Moreover, limited drug penetration in 3D cultures promotes slow-cycling, cancer stem cell-like subpopulations via increased efflux pump activity and anti-apoptotic programs (Velliou et al., 2020; Reynolds et al., 2017). Accordingly, differences between 2D and 3D responses may be influenced by 3D-associated diffusion gradients and contact-mediated signaling, supporting the use of 3D models as a complementary platform for drug evaluation. In the future, the use of this model with other molecules,

particularly other CDK4/6 inhibitors, or in combination therapies will contribute to understanding resistance mechanisms and developing more effective clinical protocols.

Our results showed that Abemaciclib induced concentration-dependent morphological changes in the cell line. While F-actin filaments showed a regular and homogeneous distribution in the cytoplasm of the control group, thickening and an increase in cellular protrusions were observed at 10 μ M Abemaciclib. This specific phenotype may be consistent with a non-canonical signaling axis where CDK4 inhibition has been reported to prevent the phosphorylation of MYO9B (a RhoGAP), potentially leading to increased RhoA activity and subsequent stress fiber bundling via the ROCK pathway (Parashar et al., 2025; Guan et al., 2023; Croft & Olson, 2006). Conversely, a significant loss of filaments and clarity of cell borders were observed at 20 μ M. This progressive disorganization may involve the additional off-target inhibition of DYRK1A, a kinase crucial for actin stability and N-WASP regulation, which abemaciclib has been reported to inhibit at higher concentrations (Kaltheuner et al., 2021; Dowjat et al., 2019; Park & Chung, 2013). Furthermore, these structural alterations mirror the morphological expansion associated with therapy-induced senescence and geroconversion, suggesting that the cells may be entering a non-proliferative yet structurally unstable state (Klein et al., 2018; Wander et al., 2022; Torres-Guzmán et al., 2017; Gleason et al., 2024). These mechanistic interpretations remain hypothetical, as no direct pathway assays were performed in this study. This indicates that the morphological integrity of the cells was compromised and the skeletal structure took on a disorganized appearance. The disruption of the F-actin network, which is critical for cell migration and invasion, by Abemaciclib is consistent with the mechanisms of action reported for other anticancer agents in MDA-MB-231 cells. Our findings also align with a recent study by Carney et al. (2024), which reported similar F-actin disruption in MDA-MB-231 cells treated with Eyes Absent (EYA) tyrosine phosphatase enzyme -sensitive peptides and doxorubicin (Carney et al., 2024). The F-actin loss obtained with Abemaciclib, consistent with studies in the literature, suggests that it may influence migration-related phenotypes; however, dedicated functional assays (e.g., migration/invasion) would be required to confirm this interpretation.

Abemaciclib suppresses the proliferation of MDA-MB-231 cells in a concentration-dependent manner and induces phase arrest. Consistent with the mechanism by which CDK4/6 inhibitors primarily stop cells in the G0/G1 phase by preventing the phosphorylation of the Rb protein (Zhou et al., 2020; Sherr et al., 2016), the application of 10 μ M Abemaciclib accumulated a large proportion of cells (45.11%) in the G0/G1 phase. This G0/G1 accumulation confirms previous findings reported for CDK4/6 inhibitors in the same cell line (Ozman et al., 2019; Pesch et al., 2022) and in the MCF-

7 cell line in another study by our team (Tuncay, 2024). The most striking finding of this experiment is the change observed in the cell cycle distribution at the higher concentrations. With the application of 20 μ M Abemaciclib, the proportion of cells arrested in the G0/G1 phase decreased significantly (19.35%), while the number of cells arrested in the G2/M phase increased (44.05%). This situation also aligns with the findings of Ozman et al. (2019) and suggests that at high concentrations, the drug may act not only through CDK4/6 inhibition but also through additional mechanisms that block the G2/M phase. In a study by Goel et al. (2018), it was stated that although CDK4/6 inhibitors primarily affect cells by stopping them in the G1 phase, these inhibitors could also affect cell biology through different mechanisms (Goel et al., 2018). The potential mechanisms underlying this observed G2/M phase arrest may draw parallels with the action pathways of Doxorubicin, which was used as a positive control. In a study by Mehraj et al. in 2022, Doxorubicin inhibited the topoisomerase II enzyme, causing double-strand breaks in DNA (Mehraj et al., 2022). Abemaciclib induces G2/M arrest at high concentrations indicates that the drug may trigger other pathways, such as the DNA damage response. For this reason, to fully elucidate the multifaceted mechanisms of action of Abemaciclib, especially its effects at clinically significant high concentrations, more detailed investigation of biological mechanisms such as the DNA damage response and apoptotic processes may also be required.

As a meaningful contribution, this study establishes and characterizes MDA-MB-231 spheroids using the 3D Petri Dish® system and provides a practical workflow for evaluating drug responses in a tumor-like 3D context. Furthermore, this model offers a robust platform for studying the behavior of aggressive tumor cells under 3D conditions and may serve as a useful reference for future academic and industrial drug screening studies.

Conclusion

These findings underline the importance of incorporating 3D tumor models in preclinical studies to improve the physiological relevance of in vitro drug testing and better reflect tumor-like architecture. In TNBC, where treatment options remain limited, the present results support the evaluation of Abemaciclib in both 2D and 3D settings and highlight that drug responses in spheroid cultures can differ over time, emphasizing the value of extended time-course assessments in 3D models.

This study has certain limitations. First, only one TNBC cell line (MDA-MB-231) was employed, and the results may not fully represent the heterogeneity of TNBC. Second, while cytoskeletal changes and cell cycle alterations were observed, the underlying molecular mechanisms, such as apoptotic signaling and DNA damage pathways, were not investigated in detail.

Third, the tested concentration range in 3D cultures limited within-range IC₅₀ estimation at later time points, and expanded dose panels and complementary endpoints would strengthen interpretation. Finally, *in vivo* validation is required to confirm the translational relevance of the findings. Future studies should investigate the use of Abemaciclib in combination with standard chemotherapeutics, targeted agents, or immunotherapies in 3D spheroid and organoid models to better simulate clinical regimens. Such approaches could help identify synergistic interactions and overcome resistance. Overall, this approach provides a physiologically relevant 3D platform for evaluating therapeutic agents, helping to bridge the translational gap between *in vitro* assays and *in vivo* studies.

Ethical Statement

This research did not involve human participants, human data, or live vertebrate animals. All experiments were conducted exclusively with the established human breast cancer cell line MDA-MB-231 (ATCC, HTB-26) under standard laboratory conditions. In accordance with the journal's author instructions, studies that do not include live vertebrate animals or human subjects do not require ethics committee approval; therefore, ARRIVE guidelines and Directive 2010/63/EU (or IACUC) are not applicable to this work. All procedures complied with institutional biosafety practices.

Funding Information

This research was financially supported by The Hacettepe University Scientific Research Projects Coordination Unit provided funding under the Project number FHD-2023-20610 (to AKS). Additional support was received from the Scientific and Technological Research Council of Türkiye (TÜBİTAK) through the Department of Science Fellowships and Grant Programmes (BİDEB) 2210-A National MSc/MA Scholarship Program (to CS) and TÜBİTAK 2209-A University Student Research Project Support Program.

Author Contributions

CS: Investigation, Formal Analysis, Data Curation, Methodology, Software, Visualization, Writing- Original Draft Preparation. SÖ: Investigation, Resources, Validation, Writing - Review & Editing. AKS: Conceptualization, Project Administration, Supervision, Writing- Review & Editing

Acknowledgement

This research was financially supported by The Hacettepe University Scientific Research Projects Coordination Unit provided funding under the Project number FHD-2023-20610 (to AKS). Additional support

was received from the Scientific and Technological Research Council of Türkiye (TÜBİTAK) through the Department of Science Fellowships and Grant Programmes (BİDEB) 2210-A National MSc/MA Scholarship Program (to CS). The authors also thank to Hande Canpınar for her flow cytometry analysis and interpretation. The funders had no role in study design, data collection and analysis, decision to publish, or preparation of the manuscript.

Conflict of Interest

The authors declare that they have no known competing financial or non-financial, professional, or personal conflicts that could have appeared to influence the work reported in this paper.

References

- Anwer, M. K., Fatima, F., Ahmed, M. M., Aldawsari, M. F., Alali, A. S., Kalam, M. A., Alshamsan, A., Alkholief, M., Malik, A., Az, A., & Al-Shdefat, R. (2022). Abemaciclib-loaded ethylcellulose based nanospheres for sustained cytotoxicity against MCF-7 and MDA-MB-231 human breast cancer cells lines. *Saudi pharmaceutical journal: SPI: the official publication of the Saudi Pharmaceutical Society*, 30(6), 726–734. <https://doi.org/10.1016/j.jsps.2022.03.019>
- Arslan, G., Önkol, T., & Özçelik, A. B. (2022). Siklin bağımlı kinaz 4/6 ve inhibitörleri [Cyclin-dependent kinase 4/6 and inhibitors]. *Journal of Faculty of Pharmacy of Ankara University*, 46(1), 193–208. <https://doi.org/10.33483/jfpau.978763>
- Badea, M. A., Balas, M., Hermenean, A., Ciceu, A., Herman, H., Ionita, D., & Dinischiotu, A. (2019). Influence of Matrigel on single- and multiple-spheroid cultures in breast cancer research. *SLAS Discovery*, 24(5), 563–578. <https://doi.org/10.1177/2472555219834698>
- Badea, M. A., Balas, M., & Dinischiotu, A. (2022). Biological properties and development of hypoxia in a breast cancer 3D model generated by hanging drop technique. *Cell biochemistry and biophysics*, 80(1), 63–73. <https://doi.org/10.1007/s12013-021-00982-1>
- Blowman, K., Magalhães, M., Lemos, M. F. L., Cabral, C., & Pires, I. M. (2018). Anticancer properties of essential oils and other natural products. *Evidence-Based Complementary and Alternative Medicine*, 2018, Article 3149362. <https://doi.org/10.1155/2018/3149362>
- Bonnier, F., Keating, M. E., Wróbel, T. P., Majzner, K., Baranska, M., Garcia-Munoz, A., Blanco, A., & Byrne, H. J. (2015). Cell viability assessment using the Alamar blue assay: A comparison of 2D and 3D cell culture models. *Toxicology in Vitro*, 29(1), 124–131. <https://doi.org/10.1016/j.tiv.2014.09.014>
- Carney, E., Ghasem Zadeh Moslabeh, F., Kang, S.-Y., Bunnell, B. A., Lee, M.-Y., & Habibi, N. (2024). Self-assembling peptides induced by eyes absent enzyme to boost the efficacy of doxorubicin therapy in drug-resistant breast cancer cells. *Heliyon*, 10(14), Article e33629. <https://doi.org/10.1016/j.heliyon.2024.e33629>
- Chica-Parrado, M. R., Kim, G. M., Uemoto, Y., Napolitano, F., Lin, C. C., Ye, D., Bikorimana, E., Fang, Y., Lee, K. M., Mendiratta, S., Hanker, A. B., & Arteaga, C. L. (2024).

- Combined inhibition of CDK4/6 and AKT is highly effective against the luminal androgen receptor (LAR) subtype of triple negative breast cancer. *Cancer letters*, 604, 217219. <https://doi.org/10.1016/j.canlet.2024.217219>
- Croft, D. R., & Olson, M. F. (2006). The Rho GTPase effector ROCK regulates cyclin A, cyclin D1, and p27Kip1 levels by distinct mechanisms. *Molecular and cellular biology*, 26(12), 4612–4627. <https://doi.org/10.1128/MCB.02061-05>
- Doello, K. (2021, October 7–10). STAT3 pathway in palbociclib resistance in breast cancer cell lines and the role of inhibitors such as tocilizumab and silymarin [Conference presentation]. AACR-NCI-EORTC International Conference on Molecular Targets and Cancer Therapeutics, Virtual.
- Dubois, C., Dufour, R., Daumar, P., Aubel, C., Szczepaniak, C., Blavignac, C., Mounetou, E., Penault-Llorca, F., & Bamdad, M. (2017). Development and cytotoxic response of two proliferative MDA-MB-231 and non-proliferative SUM1315 three-dimensional cell culture models of triple-negative basal-like breast cancer cell lines. *Oncotarget*, 8(56), 95316–95331. <https://doi.org/10.18632/oncotarget.20517>
- Dowjat, K., Adayev, T., Wojda, U., Brzozowska, K., Barczak, A., Gabryelewicz, T., & Hwang, Y. W. (2019). Abnormalities of DYRK1A-Cytoskeleton Complexes in the Blood Cells as Potential Biomarkers of Alzheimer's Disease. *Journal of Alzheimer's disease : JAD*, 72(4), 1059–1075. <https://doi.org/10.3233/JAD-190475>
- Elnozahi, N. A., Abdelaziz, E. A., Helmy, M. W., & Bistawroos, A. E. (2022). Modulatory effect of sodium butyrate on the anticancer activity of abemaciclib in MDA-MB-231 human breast cancer cells. *Journal of Pharmacy and Pharmacology Research*, 7(1), 62–73. <https://doi.org/10.21203/rs.3.rs-1619486/v2>
- George, M. A., Qureshi, S., Omene, C., Toppmeyer, D. L., & Ganesan, S. (2021). Clinical and pharmacologic differences of CDK4/6 inhibitors in breast cancer. *Frontiers in Oncology*, 11, Article 693104. <https://doi.org/10.3389/fonc.2021.693104>
- Gleason, C. E., Dickson, M. A., Klein Dooley, M. E., Antonescu, C. R., Gularte-Mérida, R., Benitez, M., Delgado, J. I., Kataru, R. P., Tan, M. W. Y., Bradic, M., Adamson, T. E., Seier, K., Richards, A. L., Palafox, M., Chan, E., D'Angelo, S. P., Gounder, M. M., Keohan, M. L., Kelly, C. M., Chi, P., ... Koff, A. (2024). Therapy-Induced Senescence Contributes to the Efficacy of Abemaciclib in Patients with Dedifferentiated Liposarcoma. *Clinical cancer research : an official journal of the American Association for Cancer Research*, 30(4), 703–718. <https://doi.org/10.1158/1078-0432.CCR-23-2378>
- Goel, S., DeCristo, M. J., McAllister, S. S., & Zhao, J. J. (2018). CDK4/6 inhibition in cancer: Beyond cell cycle arrest. *Trends in Cell Biology*, 28(11), 911–925. <https://doi.org/10.1016/j.tcb.2018.07.002>
- Goel, S., Jovanović, B., Chu, X., Hughes, M., Erick, T. K., Russo, D., DiLullo, M., Wrabel, E., Jeselsohn, R., Lin, N. U., Tayob, N., Mittendorf, E., Schnitt, S., & Tolane, S. M. (2025). A Phase II Study of Abemaciclib for Patients with Retinoblastoma-Positive, Metastatic Triple-Negative Breast Cancer. *Clinical cancer research: an official journal of the American Association for Cancer Research*, 31(8), 1427–1436. <https://doi.org/10.1158/1078-0432.CCR-24-2647>
- Guan, G., Cannon, R. D., Coates, D. E., & Mei, L. (2023). Effect of the Rho-Kinase/ROCK Signaling Pathway on Cytoskeleton Components. *Genes*, 14(2), 272. <https://doi.org/10.3390/genes14020272>
- Guney Eskiler, G., Devenci Ozkan, A., Hacıefendi, A., & Bilir, C. (2022). Mechanisms of abemaciclib, a CDK4/6 inhibitor, induced apoptotic cell death in prostate cancer cells in vitro. *Translational Oncology*, 15(1), Article 101243. <https://doi.org/10.1016/j.tranon.2021.101243>
- Habanjar, O., Diab-Assaf, M., Caldefie-Chezet, F., & Delort, L. (2021). 3D cell culture systems: Tumor application, advantages, and disadvantages. *International Journal of Molecular Sciences*, 22(22), Article 12200. <https://doi.org/10.3390/ijms222212200>
- He, J., Liu, S., Zhang, S., Gao, Q., Zhu, L., Xu, N., Hu, Z., Zhang, X., Ma, S., Wang, X., Liu, B., & Liu, W. (2025). Targeted degradation of CDK4/6 by LA-CB1 inhibits EMT and suppresses tumor growth in orthotopic breast cancer. *Scientific Reports*, 15(1), Article 7605. <https://doi.org/10.1038/s41598-025-92494-8>
- Imamura, Y., Mukohara, T., Shimono, Y., Funakoshi, Y., Chayahara, N., Toyoda, M., Kiyota, N., Takao, S., Kono, S., Nakatsura, T., & Minami, H. (2015). Comparison of 2D- and 3D-culture models as drug-testing platforms in breast cancer. *Oncology reports*, 33(4), 1837–1843. <https://doi.org/10.3892/or.2015.3767>
- Inao, T., Kotani, H., Iida, Y., Kartika, I. D., Okimoto, T., Tanino, R., Shiba, E., & Harada, M. (2019). Different sensitivities of senescent breast cancer cells to immune cell-mediated cytotoxicity. *Cancer Science*, 110(9), 2690–2699. <https://doi.org/10.1111/cas.14116>
- Jensen, C., & Teng, Y. (2020). Is it time to start transitioning from 2D to 3D cell culture? *Frontiers in Molecular Biosciences*, 7, Article 33. <https://doi.org/10.3389/fmolb.2020.00033>
- Kapaczyńska, M., Kolenda, T., Przybyła, W., Zajączkowska, M., Teresiak, A., Filas, V., Ibbs, M., Bliźniak, R., Łuczewski, Ł., & Lamperska, K. (2018). 2D and 3D cell cultures - a comparison of different types of cancer cell cultures. *Archives of Medical Science*, 14(4), 910–919. <https://doi.org/10.5114/aoms.2016.63743>
- Kaltheuner, I. H., Anand, K., Moecking, J., Düster, R., Wang, J., Gray, N. S., & Geyer, M. (2021). Abemaciclib is a potent inhibitor of DYRK1A and HIP kinases involved in transcriptional regulation. *Nature communications*, 12(1), 6607. <https://doi.org/10.1038/s41467-021-26935-z>
- Klein, M. E., Kovatcheva, M., Davis, L. E., Tap, W. D., & Koff, A. (2018). CDK4/6 Inhibitors: The Mechanism of Action May Not Be as Simple as Once Thought. *Cancer cell*, 34(1), 9–20. <https://doi.org/10.1016/j.ccell.2018.03.023>
- Lehmann, B. D., Bauer, J. A., Chen, X., Sanders, M. E., Chakravarthy, A. B., Shyr, Y., & Pietenpol, J. A. (2011). Identification of human triple-negative breast cancer subtypes and preclinical models for selection of targeted therapies. *Journal of Clinical Investigation*, 121(7), 2750–2767. <https://doi.org/10.1172/JCI45014>
- McGuire, A., Lowery, A. J., Kell, M. R., Kerin, M. J., & Sweeney, K. J. (2017). Locoregional recurrence following breast cancer surgery in the trastuzumab era: A systematic review by subtype. *Annals of Surgical Oncology*, 24(11), 3124–3132. <https://doi.org/10.1245/s10434-017-6021-1>
- Mehraj, U., Mir, I. A., Hussain, M. U., Alkhanani, M., Wani, N. A., & Mir, M. A. (2022). Adapalene and doxorubicin

- synergistically promote apoptosis of TNBC cells by hyperactivation of the ERK1/2 pathway through ROS induction. *Frontiers in Oncology*, 12, Article 938052. <https://doi.org/10.3389/fonc.2022.938052>
- Merino Bonilla, J. A., Torres Tabanera, M., & Ros Mendoza, L. H. (2017). Breast cancer in the 21st century: from early detection to new therapies. El cáncer de mama en el siglo XXI: de la detección precoz a los nuevos tratamientos. *Radiología*, 59(5), 368–379. <https://doi.org/10.1016/j.rx.2017.06.003>
- Minchinton, A. I., & Tannock, I. F. (2006). Drug penetration in solid tumours. *Nature Reviews Cancer*, 6(8), 583–592. <https://doi.org/10.1038/nrc1893>
- Nehme, J., Maassen, S., Bravaccini, S., Zaroni, M., Gianni, C., De Giorgi, U., Soto-Gamez, A., Altulea, A., Gheorghe, T., Wang, B., & Demaria, M. (2025). Pharmacological CDK4/6 inhibition promotes vulnerability to lysosomotropic agents in breast cancer. *The EMBO journal*, 44(7), 1921–1942. <https://doi.org/10.1038/s44318-025-00371-x>
- Olive, P. L., & Durand, R. E. (1994). Drug and radiation resistance in spheroids: Cell contact and kinetics. *Cancer Metastasis Reviews*, 13(2), 121–138. <https://doi.org/10.1007/BF00689632>
- Ozman, Z., Guney Eskiler, G., & Sekeroglu, M. R. (2021). In vitro therapeutic effects of abemaciclib on triple-negative breast cancer cells. *Journal of Biochemical and Molecular Toxicology*, 35(9), Article e22858. <https://doi.org/10.1002/jbt.22858>
- Öztürk, S., Demir, M., Koçkaya, E. A., Karaaslan, C., & Süloğlu, A. K. (2024). Establishment of a 3D multicellular placental microtissues for investigating the effect of antidepressant vortioxetine. *Reproductive toxicology (Elmsford, N.Y.)*, 123, 108519. <https://doi.org/10.1016/j.reprotox.2023.108519>
- Parashar, K., Simo Riudalbas, L., Ravera, A., Prieto-Baños, S., Moi, D., Drake, B. F., Shi, J., Geller, S., Dessimoz, C., & Fantner, G. E. (2025, August 8). *CDK4 restricts triple-negative breast cancer cell migration via phosphorylation-driven activation of Myo9b RhoGAP function*. bioRxiv. <https://doi.org/10.1101/2025.08.06.668850>
- Parinyanitikul, N., Sungkasubun, P., Thanakit, V., Manasayakorn, S., Raiyawa, T., & Sriuranpong, V. (2019). Prevalence of Retinoblastoma Protein Loss in Thai Women with Triple-Negative Breast Cancer. *Journal of the Medical Association of Thailand*, 102(1), 19–27.
- Park, J., & Chung, K. C. (2013). New Perspectives of Dyrk1A Role in Neurogenesis and Neuropathologic Features of Down Syndrome. *Experimental neurobiology*, 22(4), 244–248. <https://doi.org/10.5607/en.2013.22.4.244>
- Pesch, A. M., Hirsh, N. H., Michmerhuizen, A. R., Jungles, K. M., Wilder-Romans, K., Chandler, B. C., Liu, M., Lerner, L. M., Nino, C. A., Ward, C., Cobain, E. F., Lawrence, T. S., Pierce, L. J., Rae, J. M., & Speers, C. W. (2022). RB expression confers sensitivity to CDK4/6 inhibitor-mediated radiosensitization across breast cancer subtypes. *JCI Insight*, 7(3), Article e154402. <https://doi.org/10.1172/jci.insight.154402>
- Reynolds, D. S., Tevis, K. M., Blessing, W. A., Colson, Y. L., Zaman, M. H., & Grinstaff, M. W. (2017). Breast Cancer Spheroids Reveal a Differential Cancer Stem Cell Response to Chemotherapeutic Treatment. *Scientific reports*, 7(1), 10382. <https://doi.org/10.1038/s41598-017-10863-4>
- Sant, S., & Johnston, P. A. (2017). The production of 3D tumor spheroids for cancer drug discovery. *Drug Discovery Today: Technologies*, 23, 27–36. <https://doi.org/10.1016/j.ddtec.2017.03.002>
- Scope, A., Essat, M., Pandor, A., Rafia, R., Ward, S. E., Wyld, L., Cross, S., & Woods, H. B. (2017). GENE EXPRESSION PROFILING AND EXPANDED IMMUNOHISTOCHEMISTRY TESTS TO GUIDE SELECTION OF CHEMOTHERAPY REGIMENS IN BREAST CANCER MANAGEMENT: A SYSTEMATIC REVIEW. *International journal of technology assessment in health care*, 33(1), 32–45. <https://doi.org/10.1017/S0266462317000034>
- Sharaky, M., El Kiki, S. M., Effat, H., & Mansour, H. H. (2025). Effect of palliative radiotherapy and cyclin-dependent kinase 4/6 inhibitor on breast cancer cell lines. *Naunyn-Schmiedeberg's Archives of Pharmacology*. Advance online publication. <https://doi.org/10.1007/s00210-025-03878-6>
- Sherr, C. J., Beach, D., & Shapiro, G. I. (2016). Targeting CDK4 and CDK6: From discovery to therapy. *Cancer Discovery*, 6(4), 353–367. <https://doi.org/10.1158/2159-8290.CD-15-0894>
- Sørli, T., Perou, C. M., Tibshirani, R., Aas, T., Geisler, S., Johnsen, H., Hastie, T., Eisen, M. B., van de Rijn, M., Jeffrey, S. S., Thorsen, T., Quist, H., Matese, J. C., Brown, P. O., Botstein, D., Lønning, P. E., & Børresen-Dale, A. L. (2001). Gene expression patterns of breast carcinomas distinguish tumor subclasses with clinical implications. *Proceedings of the National Academy of Sciences*, 98(19), 10869–10874. <https://doi.org/10.1073/pnas.191367098>
- Torres-Guzmán, R., Calsina, B., Hermoso, A., Baquero, C., Alvarez, B., Amat, J., McNulty, A. M., Gong, X., Boehnke, K., Du, J., de Dios, A., Beckmann, R. P., Buchanan, S., & Lallena, M. J. (2017). Preclinical characterization of abemaciclib in hormone receptor positive breast cancer. *Oncotarget*, 8(41), 69493–69507. <https://doi.org/10.18632/oncotarget.17778>
- Tuncay, C. (2024). *Abemaciclib'in 3B Petri Dish yöntemi ile üretilen MCF-7 meme kanseri sferoidlerinin üzerine etkisi (2209-A Sonuç Raporu)*. TÜBİTAK.
- Velez, B. C., Petrella, C. P., DiSalvo, K. H., Cheng, K., Kravtsov, R., Krasniqi, D., & Krucher, N. A. (2023). Combined inhibition of ACLY and CDK4/6 reduces cancer cell growth and invasion. *Oncology Reports*, 49(2), Article 32. <https://doi.org/10.3892/or.2022.8469>
- Velliou, E., Gupta, P., Ricci, C., & Danti, S. (2020). Biomaterial-based in vitro models for pancreatic cancer. In S. C. Kundu & R. L. Reis (Eds.), *Biomaterials for 3D tumor modeling* (pp. 235–249). Elsevier. <https://doi.org/10.1016/B978-0-12-818128-7.00011-3>
- Wander, S. A., O'Brien, N., Litchfield, L. M., O'Dea, D., Morato Guimaraes, C., Slamon, D. J., & Goel, S. (2022). Targeting CDK4 and 6 in Cancer Therapy: Emerging Preclinical Insights Related to Abemaciclib. *The Oncologist*, 27(10), 811–821. <https://doi.org/10.1093/oncolo/oyac138>
- Wang, C., Tang, Z., Zhao, Y., Yao, R., Li, L., & Sun, W. (2014). Three-dimensional in vitro cancer models: A short review. *Biofabrication*, 6(2), Article 022001. <https://doi.org/10.1088/1758-5082/6/2/022001>
- Wang, H., Xu, T., & Yin, D. (2023). Emerging trends in the methodology of environmental toxicology: 3D cell culture and its applications. *Science of the Total Environment*, 857(Pt 2), Article 159501. <https://doi.org/10.1016/j.scitotenv.2022.159501>

- Wild, C. P., Weiderpass, E., & Stewart, B. W. (Eds.). (2020). *World cancer report: Cancer research for cancer prevention*. International Agency for Research on Cancer. <https://publications.iarc.fr/586>
- Zhang X. (2023). Molecular Classification of Breast Cancer: Relevance and Challenges. *Archives of pathology & laboratory medicine*, 147(1), 46–51. <https://doi.org/10.5858/arpa.2022-0070-RA>
- Zhou, Y., Li, Y., Shen, J., Li, J., & Li, X. (2020). Abemaciclib induces apoptosis in cardiomyocytes by activating the Hippo signaling pathway. *Acta biochimica et biophysica Sinica*, 52(8), 875–882. <https://doi.org/10.1093/abbs/gmaa066>

ACCEPTED MANUSCRIPT

Table 1. IC₅₀ values (μM) of Abemaciclib in 2D and 3D culture

Abemaciclib IC₅₀ (μM)		
Incubation Time	IC₅₀ (μM) in 2D Culture	IC₅₀ (μM) in 3D Culture
24 h	21.471 μM	37.126 μM
48 h	20.001 μM	41.073 μM
72 h	19.320 μM	46.205 μM

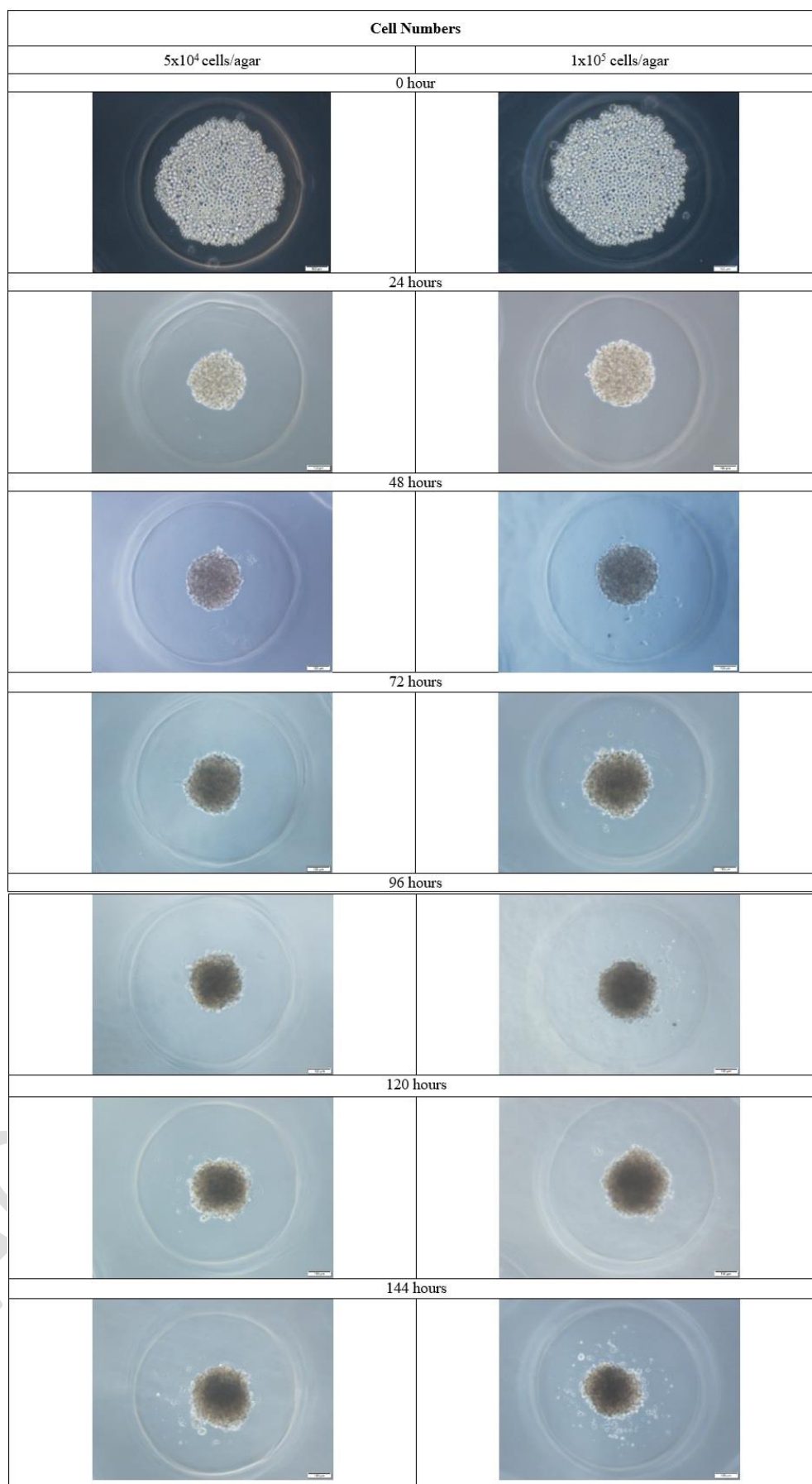


Figure 1. Inverted microscopic images of spheroids over 6 days (Scale bar: 100 μm).

Diameter Measurement in MDA-MB-231 Spheroids

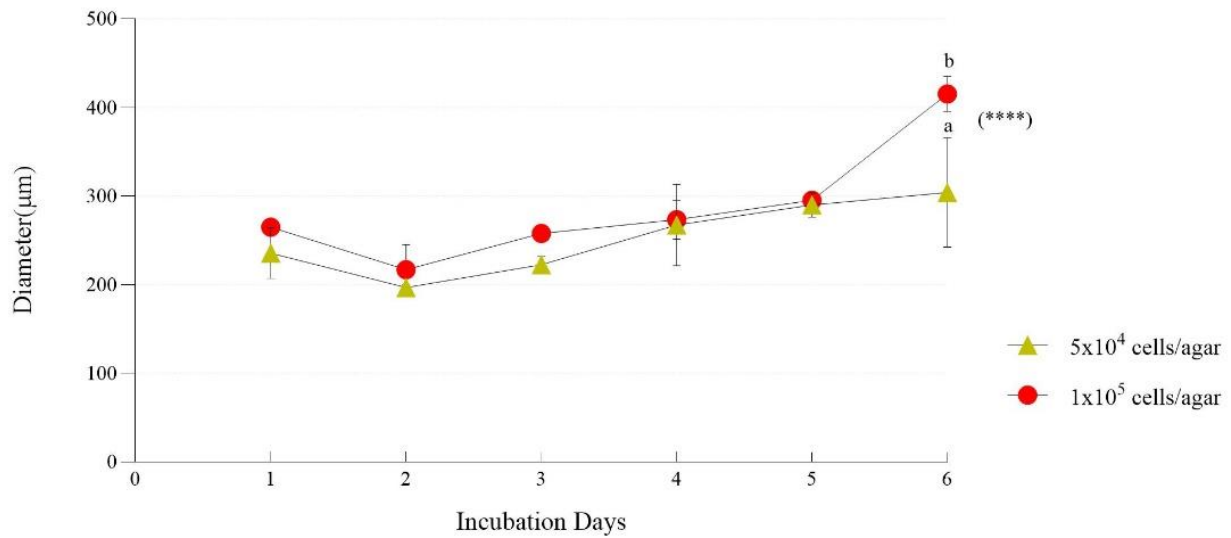


Figure 2. Diameter measurements of MDA-MB-231 spheroids in 3D culture across 5×10^4 and 1×10^5 cells/agar groups over a 6-day incubation period. Data are expressed as mean \pm SD ($N=3$). Two-way ANOVA revealed that both the incubation period ($P < 0.0001$) and initial cell concentration ($P=0.0009$) had a statistically significant overall effect on spheroid diameter. Post-hoc multiple comparisons using Dunnett's test were performed to compare the mean diameter of each day against the Day 1 control group. a: Statistically significantly different from Day 1 in the 5×10^4 cells/agar group ($P=0.0217$). b: Statistically significantly different from Day 1 in the 1×10^5 cells/agar group ($P < 0.0001$). **** ($P < 0.0001$) indicates a highly significant difference between the two cell densities at Day 6.

Measurement of Spheroid Area in MDA-MB-231 Cells

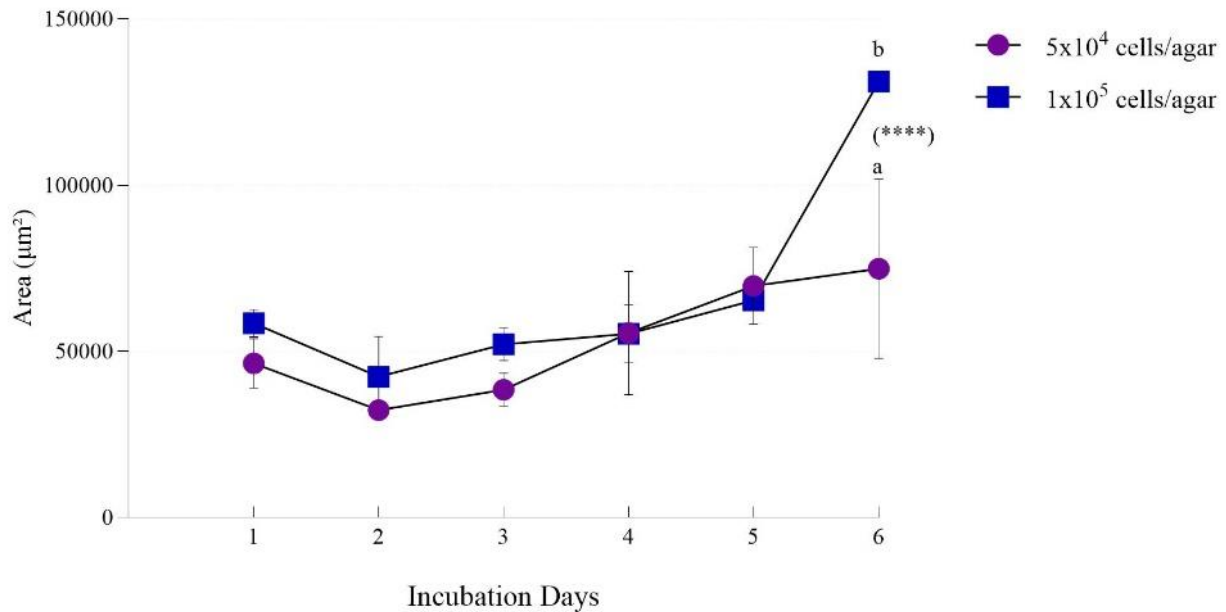


Figure 3. Area measurements of MDA-MB-231 spheroids in 3D culture across 5×10^4 and 1×10^5 cells/agar groups over a 6-day incubation period. Data are expressed as mean \pm SD ($N=3$ for all time points). Two-way ANOVA revealed that both the incubation period ($P < 0.0001$) and initial cell concentration ($P < 0.0001$) had a highly significant overall effect on spheroid area. Post-hoc multiple comparisons using Dunnett's test were performed to compare the mean area of each day against the Day 1 control group. a: Statistically significantly different from Day 1 in the 5×10^4 cells/agar group ($P = 0.0230$). b: Statistically significantly different from Day 1 in the 1×10^5 cells/agar group ($P < 0.0001$). **** ($P < 0.0001$) indicates a highly significant difference between the two cell densities at Day 6.

MDA-MB-231 2D MTS Analysis

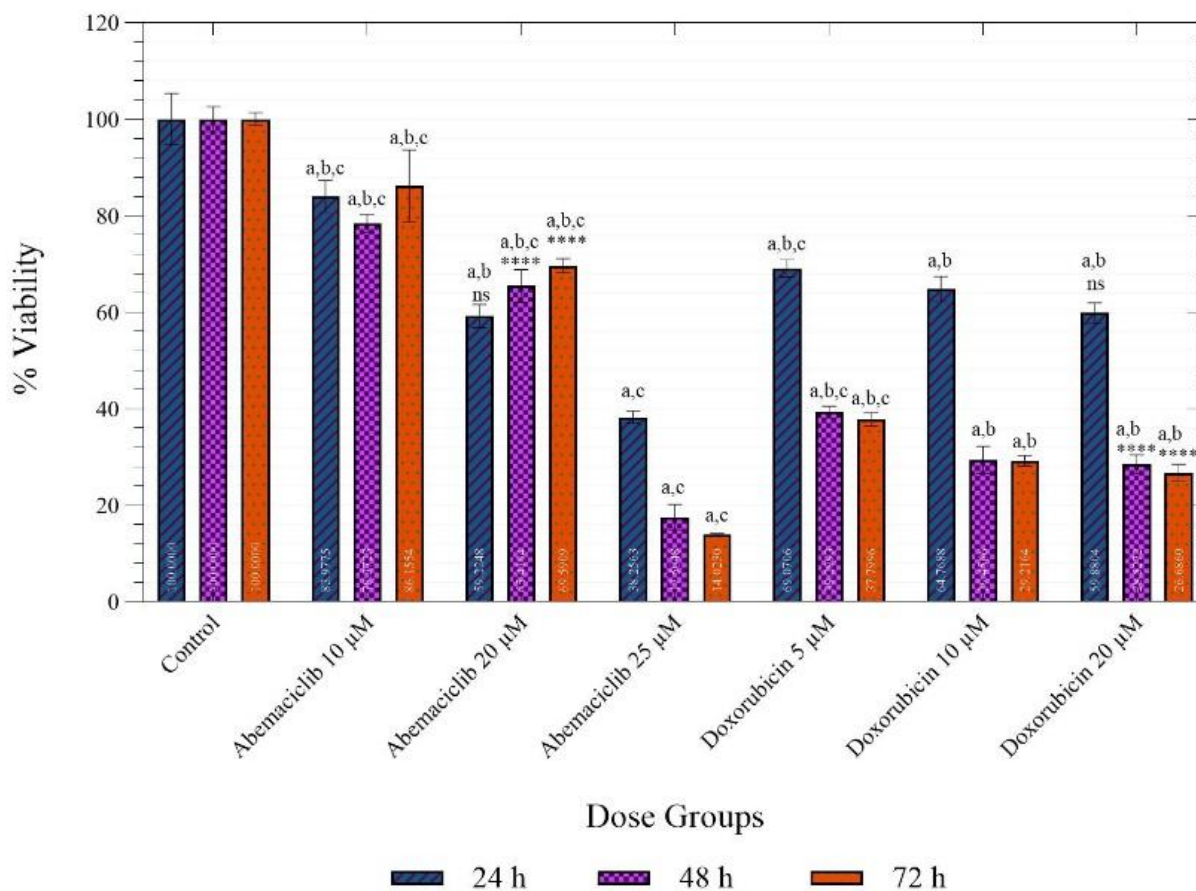


Figure 4. Cell viability of MDA-MB-231 cells in 2D culture following treatment with Abemaciclib and Doxorubicin. Cells were treated with varying concentrations of Abemaciclib (10, 20, 25 µM) and Doxorubicin (5, 10, 20 µM) for 24, 48, and 72 hours. Viability was assessed by MTS assay and data are presented as mean \pm SD ($N=3$). Statistical significance was determined using ordinary two-way ANOVA followed by Šidák's multiple comparisons test. a: Statistically significant difference compared to the control group ($P<0.0001$). b: Statistically significantly different from the Abemaciclib 25 µM group ($P\leq 0.05$). c: Statistically significantly different from the Doxorubicin 20 µM group ($P\leq 0.05$). **** ($P < 0.0001$) indicates a highly significant difference between Abemaciclib and Doxorubicin at the equivalent dose of 20 µM ns: Not significant ($P > 0.05$).

MDA-MB-231 3D MTS Analysis

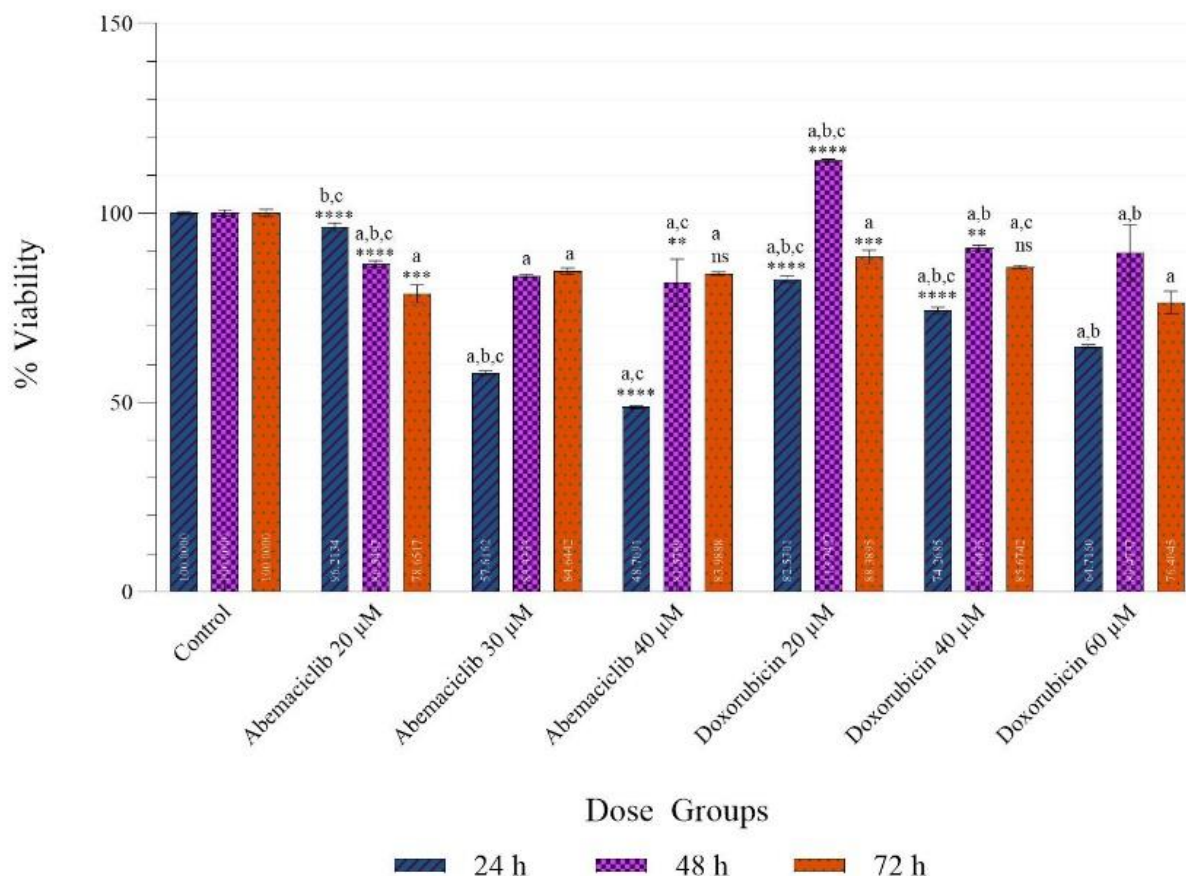


Figure 5. Cell viability of MDA-MB-231 3D spheroids following treatment with Abemaciclib and Doxorubicin. Cells were treated with varying concentrations of Abemaciclib (20, 30, 40 µM) and Doxorubicin (20, 40, 60 µM) for 24, 48, and 72 hours. Viability was assessed by MTS assay and data are presented as mean \pm SD ($N=3$). Statistical significance was determined using ordinary two-way ANOVA followed by Šídák's multiple comparisons test. a: Statistically significantly different from the control group ($P<0.0001$). b: Statistically significantly different from the Abemaciclib 40 µM group ($P\leq 0.05$). c: Statistically significantly different from the Doxorubicin 60 µM group ($P\leq 0.05$). **** ($P<0.0001$) indicates a highly significant difference between Abemaciclib and Doxorubicin at equivalent doses (20 µM and 40 µM) at 24 h, and for 20 µM at 48 h; *** ($P<0.001$) indicates a very significant difference at 72 h for 20 µM; ** ($P<0.01$) represents a significant difference at 48 h for the 40 µM dose groups; whereas ns ($P>0.05$) represents non-significance between drug types at 72 h for the 40 µM concentration groups.

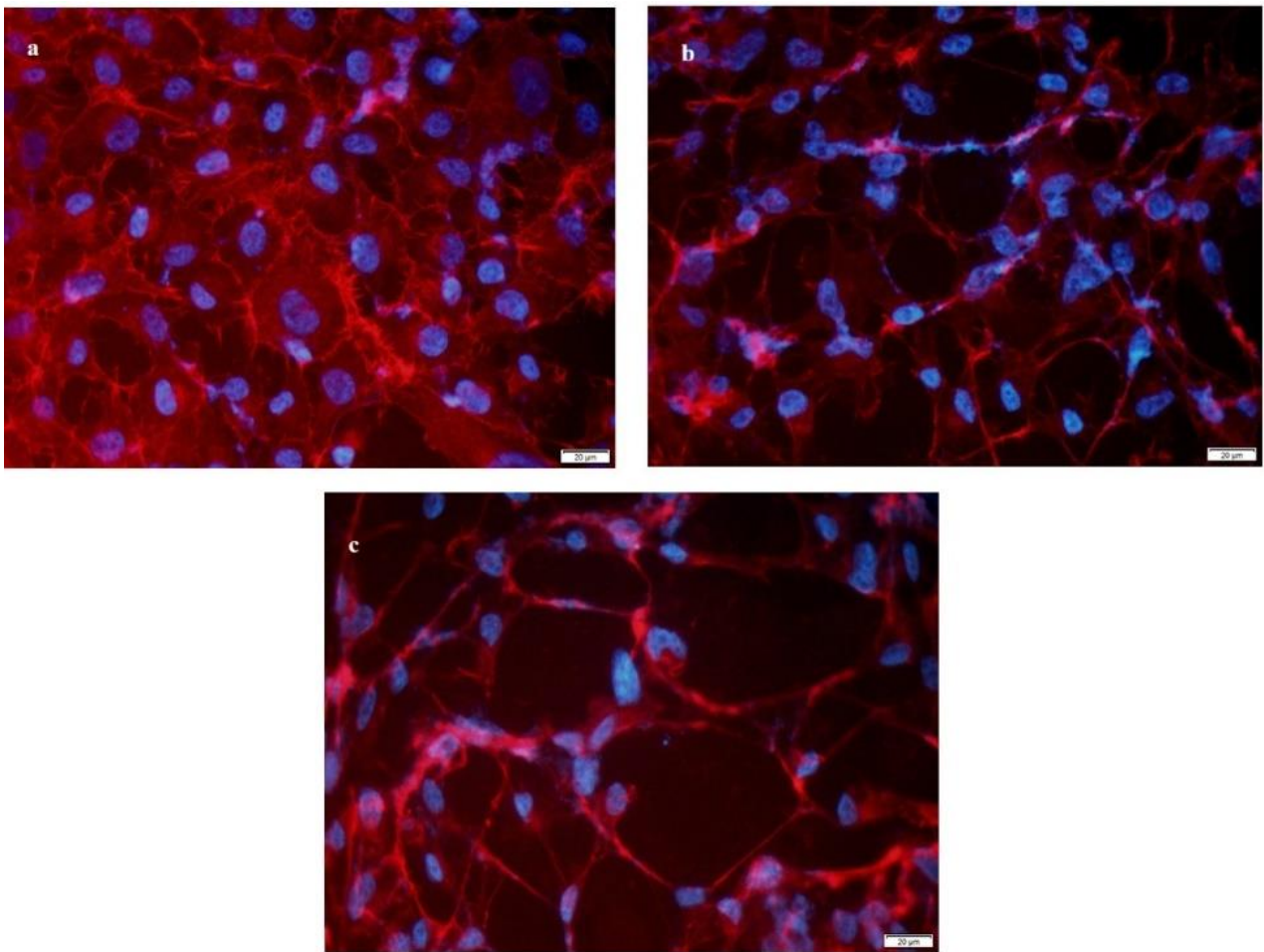


Figure 6. Representative immunofluorescent images showing F-actin distribution in MDA-MB-231 cells under different conditions: (a) Control, (b) 10 μM Abemaciclib, (c) 20 μM Abemaciclib (Scale bar: 20 μm).

ACCEPTED

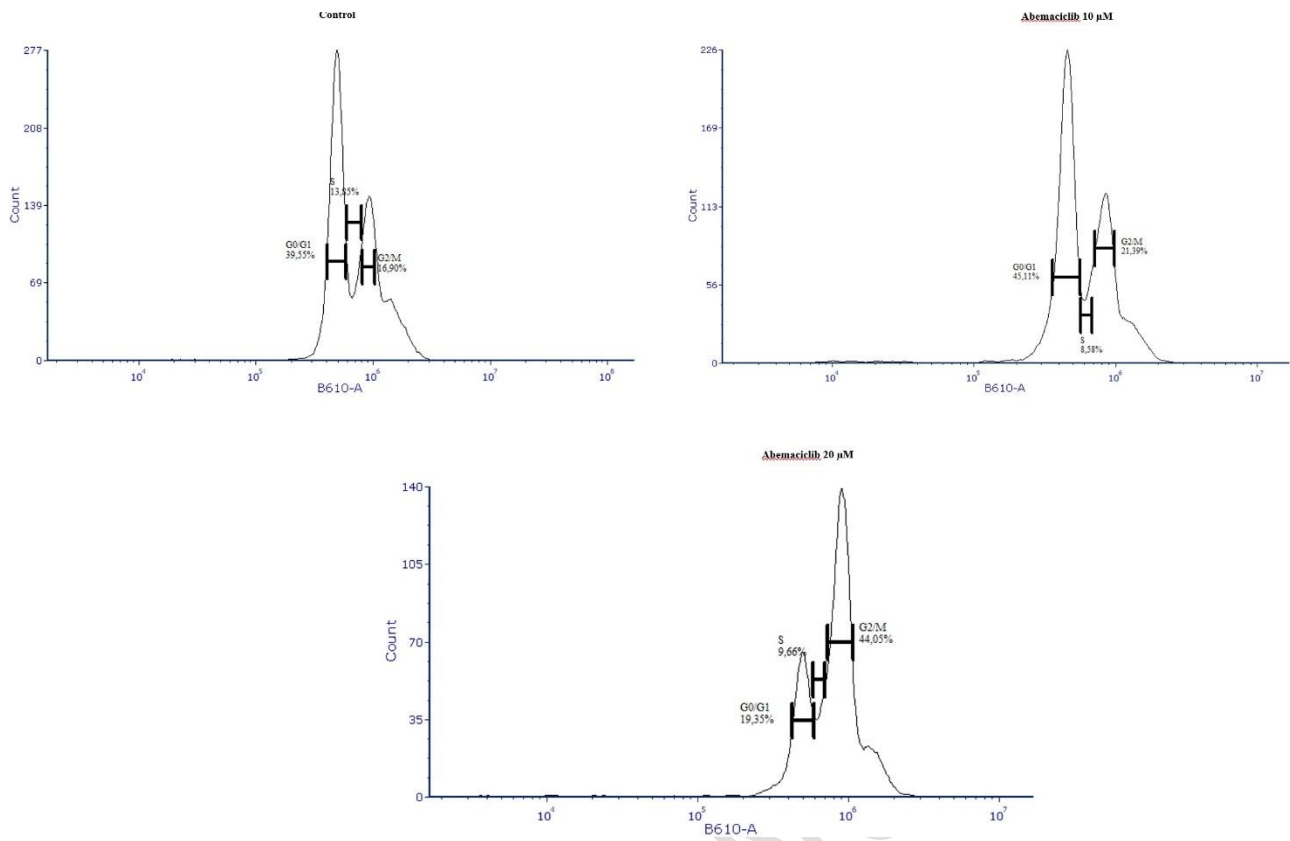


Figure 7. Flow cytometric analysis illustrating the effects of Abemaciclib treatment (10 μ M and 20 μ M) on cell cycle distribution in MDA-MB-231 cells. The percentages of cells in G0/G1, S, and G2/M phases were compared to untreated control cells.

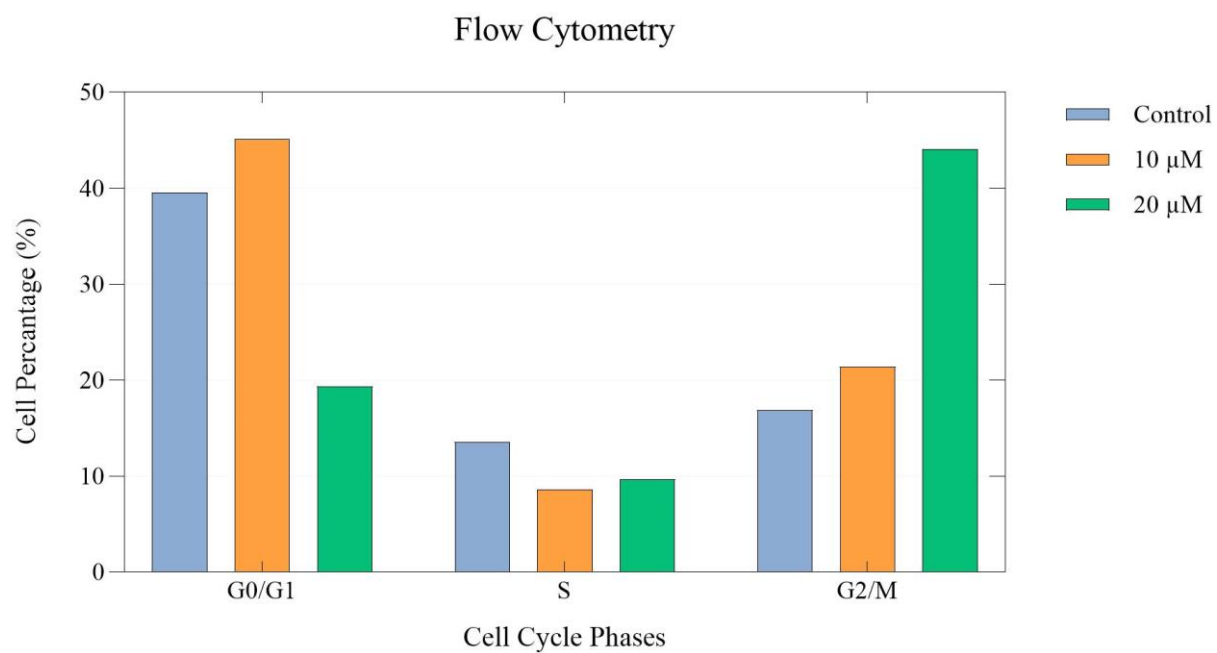


Figure 8. Flow cytometry histogram plots showing the effects of Abemaciclib treatment (10 μM and 20 μM) on cell cycle distribution in MDA-MB-231 cells.